Research Article

Construction Sequence Optimization and Settlement Control Countermeasures of Metro Tunnels Underpassing Expressway

Chengzhong Zhang [ID],[1,2] **Qiang Zhang** [ID],[1,2] **Ziming Pei** [ID],[1,2] **Zhanping Song** [ID],[1,2] **and Junbao Wang** [ID][1,2]

[1]*School of Civil Engineering, Xi'an University of Architecture and Technology, Xi'an, Shaanxi 710055, China*
[2]*Shaanxi Key Laboratory of Geotechnical and Underground Space Engineering, Xi'an, Shaanxi 710055, China*

Correspondence should be addressed to Qiang Zhang; nndsjyzq@163.com and Ziming Pei; 281083195@qq.com

The Chongqing metro line 6 underpass expressway around the city is taken as an engineering background, and the optimal excavation sequence and corresponding control countermeasures for the triangular-distributed three-line metro tunnel underpass expressway are studied. The influences of excavation sequence on the tunnel surrounding rock deformation, surrounding rock stress, supporting structure stress, plastic zone, and surface settlement are analyzed by using MIDAS/GTS NX finite element software. The numerical simulation results showed that Case 1 is the optimal excavation sequence of the metro tunnel. However, the surface settlement under the optimal excavation sequence exceeds the limit value of 30 mm, which cannot guarantee the safety of expressway traffic. On this basis, the control measure for strengthening the three-line tunnels with advanced small pipe grouting and reinforcing the middle tunnel with concrete-filled steel tube piles are proposed. Moreover, the excavation process of the metro tunnel with and without reinforcement schemes is numerically simulated. The results show that the reinforcement scheme can effectively control the surface settlement value within the limited value (16.47 mm), which is close to the maximum surface settlement of 18.31 mm after the metro tunnel excavation is completed, indicating that the proposed reinforcement scheme is beneficial to ensure the safety of metro tunnel construction and the driving safety of the expressway.

1. Introduction

Newly built metro tunnels underpassing through the upper existing buildings (structures) and traffic lines are common engineering problems in urban infrastructure construction [1–3]. During the construction of metro tunnels, it is very easy to cause large surface settlement, which will threaten the safety of existing buildings (structures) and traffic lines on the upper part [4–6]. Therefore, it is necessary to study the impact of metro tunnel construction on the existing buildings (structures) and traffic lines and the corresponding construction control countermeasures [7–9].

In order to ensure the safety of metro tunnel construction and reduce the impact on existing buildings (structures) and traffic lines, relevant scholars have conducted a lot of research studies on metro tunnel

underpassing projects and corresponding control measures [10–12]. Lu [13] used the CAESAR II software to establish the stress analysis model of Yanyingshan tunnel pipeline based on the Lantsang tunnel crossing pipeline project and studied the change law of pipeline stress state and displacement during tunnel construction. Liu et al. [14] used the MIDAS/GTS NX finite element software to analyze the impact of shield tunnel construction on the existing railway by taking Zhengzhou metro line 4 under the Longhai railway as an example. Chung et al. [15] studied the influence of continuous excavation of new metro tunnels on the stability of existing metro tunnels using numerical simulation methods and proposed the best excavation sequence and reinforcement methods to ensure the stability of metro tunnel entrances and exits. Xing et al. [16] studied the impact of precipitation and new metro excavation on existing metro

tunnels through theoretical analysis and finite element simulation and proposed groundwater treatment measures and protection schemes for existing metro tunnels. Zhang et al. [17] used real-time monitoring data to analyze the impact of the construction of a new metro tunnel on the existing tunnel, and the results showed that advanced grouting can achieve the overall uplift within the reinforced area, and jack hoisting is the key to suppressing the settlement. Lai et al. [18] proposed a method for predicting the surface settlement caused by the construction of a metro double tunnel underneath the existing tunnel based on the comprehensive analysis of the coupling effect of the new tunnel, soil, and existing tunnel, with the effectiveness of the method verified by engineering examples. Jin et al. [19] studied the influence of shield tunnels on the surface settlement of existing tunnels during the construction process based on the monitoring data of a large number of underpass metro tunnel construction cases and pointed out that the longitudinal additional stress of the existing tunnels is the main reason which caused the tunnel lining water seepage and structure damage Wu et al. [20] used a combination of the numerical simulation and model test to study the influence of the construction method of a new metro tunnel on the deformation and stability of the existing structure. Zhou et al. [21] established a theoretical model of deformation prediction caused by a new tunnel underpassing an existing tunnel based on the Peck formula and used the Beijing metro line 10 underpassing metro line 1 as an engineering case to verify the rationality of the model. Castaldo et al. [22] used the results of the numerical model of the boundary value problem and proposed a simplified probabilistic method to evaluate the impact of the new tunnel excavation on the adjacent existing buildings. Lai et al. [6] studied the influence of shield tunnel construction on the settlement characteristics of existing tunnels based on on-site monitoring data and numerical simulation software, and the results showed that the deformation of existing tunnels caused by shield tunneling was mainly the vertical settlement, accompanied by the torsion deformation. At present, most of the two-line or three-line metro tunnels under construction and already built are in parallel in a straight line, while the triangular-distributed three-line tunnel section is still rare in metro construction [23–26]. The tunnel structure of this section is more complicated. Different construction methods and excavation sequence differences will have an important impact on the tunnel support structure, surrounding rock stress, deformation characteristics, surface settlement, upper existing buildings (structures), and traffic routes [27–32]. In the case in which the construction method is determined, determining the optimal excavation sequence is of great significance for reducing the disturbance of the surrounding rock and ensuring the stability of the tunnel structure, upper existing buildings (structures), and traffic safety [33–37].

Based on the Chongqing metro tunnel line 6 underpassing through the expressway around the city, the MIDAS/GTS NX numerical simulation software is used to simulate the surrounding rock deformation, supporting structure stress distribution, and surface settlement of the metro tunnel under different excavation sequences, and the

optimal excavation sequence is determined. On this basis, the control measure for strengthening the three-line tunnels with advanced small pipe grouting and reinforcing the middle tunnel with concrete-filled steel tube piles is proposed, and the numerical simulation of the metro tunnel excavation process with and without reinforcement schemes is carried out.

2. Project Overview and Construction Difficulties

2.1. Project Overview. Chongqing metro line 6 from Qingxi River to Liujiayuanzi section of the two-lane tunnel (left and right lines) and Caojiawan access section right line (middle line), a total of three tunnels at K17 + 520 ~ K17 + 960 (YCK0+380 ~ YCK0+870), with the mileage section underpassing through the expressway around the city and the service area. The excavation section of this part of the tunnel is about 7.11 m high and 7.06 m wide, and the section is underpassing through the fill area. In the mileage section of K17 + 680 ~ K17 + 720, these three tunnels are distributed in a triangle and underpassing through the expressway around the city. The intersection angle between the axis of the metro tunnel and axis of the expressway is about 69°, underpassing distance is about 40 m, overlying fill range is about 135 m, and minimum distance from the tunnel vault to the expressway around the city is about 7.2 m. The schematic plan and cross-sectional distribution diagram for the metro tunnel underpassing through the expressway around the city are shown in Figures 1 and 2, respectively.

2.2. Engineering Geological Conditions and Hydrogeological Conditions. The metro tunnel stratum mainly includes the Quaternary Holocene fill layer (Q_4^{ml}), Quaternary Holocene residual slope clay (Q_4^{el+dl}), Jurassic Middle Shaximiao Formation (J_2^s) sandstone, and sandy mudstone. The Quaternary Holocene system fill layer (Q_4^{ml}) is mainly plain fill, distributed in the artificial reconstruction area along the tunnel, with a maximum thickness of about 28.3 m. The Quaternary Holocene residual slope cohesive soil (Q_4^{el+dl}) is mainly silty clay, distributed in the nonartificially modified area along the tunnel; the thickness of the soil layer is about 0.2–5.2 m, and the local thickness can reach 8.5 m. The Middle Jurassic Shaximiao Formation (J_2^s) is mainly composed of moderately weathered sandstone and sandy mudstone; the rock mass is not developed with cracks, and the rock mass is relatively complete, which belongs to class III surrounding rock; however, the sandy mudstone in some sections has a relatively large sand content and large strength variability and belongs to the V-level surrounding rock.

The groundwater along the tunnel is mainly Quaternary loose layer pore water and bedrock fissure water. The loose layer pore water is mainly distributed in the artificial fill layer and residual slope layer. The amount of water is small, and it is greatly affected by climate and seasonal changes. Bedrock fissure water is mainly distributed in the strong weathering zone of the shallow bedrock and the middle and

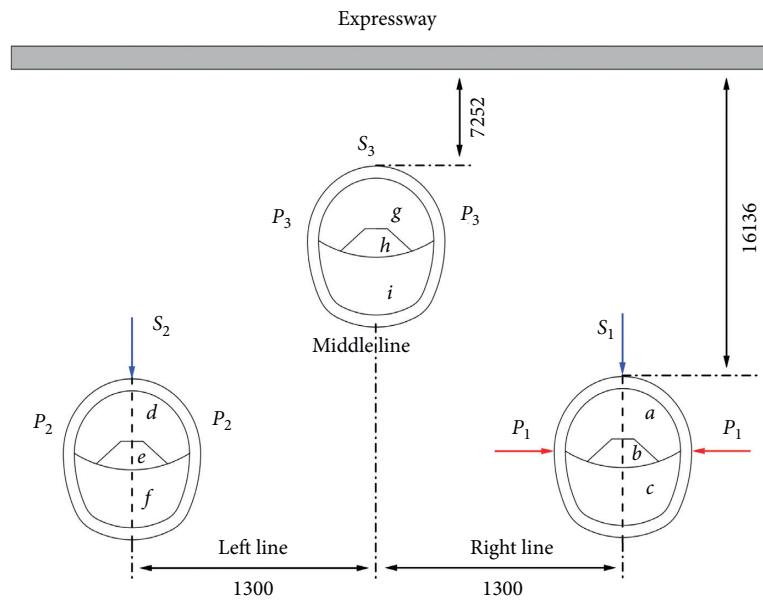FIGURE 1: The schematic diagram for the underpassing.

FIGURE 2: The cross-section distribution map for the metro tunnel underpassing through the expressway (unit: mm).

lower-middle-thick massive bedrock fissures. The amount of water is small, and it is greatly affected by seasonality.

2.3. Engineering Difficulties

(1) Most of the two-line or three-line metro tunnels currently under construction and already built are distributed in parallel in a straight line. However, in this project, the three tunnels are distributed in a triangular shape, that is, the middle tunnel is located directly above the middle point of the left and right tunnels, and the arch bottom of the middle tunnel is higher than the vaults of the left and right tunnels (as shown in Figure 2). This type of distribution of tunnel sections is still rare in metro tunnel construction. In particular, the maximum distance between the vault of the tunnel in the middle of the

section and the ground surface is only 15 m, which is a shallow tunnel. Therefore, the determination of a reasonable excavation plan, excavation sequence, and construction parameters have become the key issues for the safe and rapid construction of this project.

(2) The underground excavation is carried out under the condition of backfilled soil. Due to the poor self-stability of the surrounding rock of the tunnel, the surrounding rock should be reinforced in advance to ensure the safety and stability of the excavation section before tunnel excavation in this layer.

(3) The expressway around Chongqing city where the new metro tunnels underpassing in this project are in operation. To ensure driving safety, the surface settlement should be strictly controlled during the tunnel construction. Therefore, selecting appropriate

control countermeasures to strictly control the surface settlement is the most difficult point of this project.

3. The Construction Sequence Optimization of the Triangle-Distributed Three-Line Metro Tunnels Underpassing through the Expressway

The section structure of the triangular-distributed three-line metro tunnels is more complicated. Different construction methods and different excavation sequences will have an important impact on the tunnel support structure, surrounding rock stress, deformation characteristics, and surface settlement. Especially when the construction method is determined, determining the optimal excavation sequence is of great significance for reducing the disturbance of the surrounding rock and ensuring the stability of the surrounding rock of the tunnel. The MIDAS/GTS NX finite element software is used in this paper to carry out numerical simulations of different excavation sequences for Chongqing metro line 6 underpassing the expressway project. And, the most excellent tunnel excavation sequence scheme is determined by comparing and analyzing the numerical simulation results under different schemes.

3.1. Numerical Calculation Model and Relevant Parameters. In the numerical simulation, according to the geological survey of the section of the underpass expressway, since the geological conditions of the K17 + 720 section are relatively complicated, this section is selected as the research object, with the two bench-cut method of core soil reserved on the upper step. In order to simplify the calculation, each rock and soil layer is regarded as a horizontal distribution, and it is regarded as an isotropic homogeneous elastic material. According to the actual project, the center line tunnel is completely in the backfilled stratum, and the left and right line tunnels are in the silty clay and sandy mudstone stratum. Since deep-well point precipitation has been used before tunnel excavation, there is no groundwater in the construction interval, so the influence of groundwater is ignored in the numerical simulation. At the same time, it is assumed that the initial stress is only the self-weight stress of each rock and soil layer. When meshing, the rock and soil layers are divided by 2D units, and the Mohr–Coulomb constitutive model is selected as the constitutive model of the rock and soil layers. 1D beam elements are used to divide the supporting structure and central diaphragm, and an elastic model is selected as the constitutive model of the supporting structure and central diaphragm; the model is divided into 1921 nodes and 2047 elements.

The excavation of the tunnel will cause deformation of the surrounding rock and soil, and its influence range is generally 3 to 5 times that of the tunnel diameter. Combined with the actual project, the dimensions of the numerical model in the *X*-axis and *Y*-axis directions are 80 m and 46.4 m, respectively. The *X*-axis direction is horizontal and perpendicular to the tunnel axis, and the *Y*-axis direction is the vertical direction. The upper surface is a free surface, and the left side, right side, and lower part are displacement constraints. The finite element model is shown in Figure 3.

According to the on-site geological survey report, the section of the tunnel underneath the expressway is composed of artificial fill, silty clay, sandy mudstone, and sandstone from top to bottom, and the middle line tunnel is completely in the artificial fill. Most of the left and right tunnels are in sandy mudstone, and the partial vault structure is in silty clay rock. The thickness of roadbed, artificial fill layer, silty clay layer, sandy mudstone layer, and sandstone layer are 1.4 m, 15 m, 3 m, 7 m, and 20 m in order. The physical and mechanical parameters of each rock and soil layer are shown in Table 1.

All three tunnels adopt composite lining structure, and the initial supporting structure adopts C25 concrete with a thickness of 300 mm. In the tunnel support, two layers of Φ8 steel mesh with a grid spacing of 20 cm × 20 cm are used; the steel frame adopts an I28b type full-ring arrangement with a spacing of 0.5 m the secondary lining adopts C40 concrete with a thickness of 500 mm. During model analysis, the initial support structure is simulated with an elastic model. According to the Code for Design of Concrete Structures of China (GB 50010–2011), the elastic modulus of C25 concrete and steel bars are 28 GPa and 200 GPa, respectively. The elastic modulus of the primary support adopts the equivalent elastic modulus and is calculated according to Equation (1). The physical and mechanical parameters of each support are shown in Table 2.

where E is the converted elastic modulus of the initial support, E_0 is the elastic modulus of sprayed concrete, E_g is the elastic modulus of the steel bar, S_g is the cross-sectional area of the steel bar, and S_0 is the cross-sectional area of concrete.

$$E = E_0 + \frac{S_g E_g}{S_0}, \tag{1}$$

3.2. Excavation Schemes. In order to avoid the influence of time and space effects during the excavation process, the load is released three times during the tunnel construction phase, and the load release coefficients are 0.4, 0.3, and 0.3, respectively. According to the actual engineering situation of Chongqing metro line 6, the three tunnels are distributed in a triangular shape, and the two bench-cut method of core soil reserved on the upper step is adopted for construction. The construction sequence of each tunnel is given as follows (taking the tunnel on the right in Figure 1 as an example): (1) excavate the pilot tunnel *a* and then construct the primary support; (2) excavate the core soil *b* and construct the middle partition; (3) excavate the pilot tunnel *c*, construct the primary support, and remove the middle partition; (4) construct the secondary lining. According to the above-mentioned construction sequence of a single tunnel, the following three excavation schemes of the numerical simulation in this paper are proposed.

Case 1. Right line tunnel ⟶ left line tunnel ⟶ middle line tunnel.

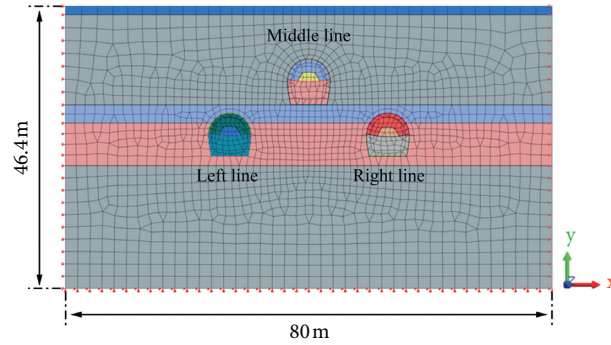Case 2. Right line tunnel ⟶ middle line tunnel ⟶ left line tunnel.

FIGURE 3: The finite element model diagram.

TABLE 1: Physical and mechanical parameters of rock and soil layers.

Type	Bulk density (kN/m³)	Internal friction angle (°)	Cohesion (kPa)	Elastic modulus (MPa)	Poisson's ratio
Roadbed	20	36	30	15	0.3
Artificial fill	20	25	5	17	0.35
Silty clay	20	10.2	20.9	20	0.23
Sandy mudstone	25.6	31.2	440	2030	0.35
Sandstone	24.7	35	2100	4260	0.14

TABLE 2: Supporting physical and mechanical parameters.

Type	Bulk density (kN/m³)	Modulus of elasticity (GPa)	Poisson's ratio	Thickness (mm)
Initial support	25	28	0.2	300
Middle partition	25	28	0.3	300
Secondary lining	25	32.5	0.2	300

Case 3. Center line tunnel ⟶ right line tunnel ⟶ left line tunnel.

3.3. Analysis of Numerical Simulation Results

3.3.1. Deformation of the Surrounding Rock and Supporting Structure. Figures 4 and 5, respectively, show the vertical and horizontal displacement cloud diagrams of the surrounding rock under different excavation schemes. It can be seen that, after the tunnel excavation is completed, the influence of different excavation schemes on the deformation of the surrounding rock is basically the same: (1) the maximum settlement values under the three excavation schemes all appear at the tunnel vault, and the maximum values are −42.13 mm, −48.04 mm, and −53.26 mm, respectively; (2) the inverted arch of the tunnel is uplifted, but due to the poor nature of the surrounding rock of the middle line tunnel, the uplift of the inverted arch is more obvious than that of the left and right line tunnels, and the maximum values under the three excavation schemes are 20.59 mm, 22.82 mm, and 12.36 mm, respectively; (3) the maximum horizontal displacements all appear on the left side of the middle line tunnel (*X*-axis negative direction), and the maximum values under the three excavation schemes are 12.36 mm, 12.36 mm, and 12.60 mm, respectively. It can be seen from the above results that compared with Cases 2 and 3, Case 1 has a more obvious effect on controlling the surrounding rock deformation of the tunnel.

In order to study the influence of the three excavation schemes on the primary support deformation of the tunnel, the vault settlement of the tunnel and haunch horizontal convergence were selected as reference values for analysis, and the layout of each monitoring point is shown in Figure 2. P_i ($i = 1$, 2, and 3) is the monitoring point of the vault settlement, and S_i ($i = 1$, 2, and 3) is the monitoring point of the haunch horizontal convergence. Table 3 shows the vault settlement value and haunch horizontal convergence value of the three tunnels under different excavation schemes. Due to the poor nature of the surrounding rock in the middle line tunnel, the vault settlement value and haunch horizontal convergence value are significantly greater than that of the left and right line tunnels. It can be seen from Table 3 that the vault settlement value of the tunnel and haunch horizontal convergence value under Case 3 are the largest, followed by Case 2, and Case 1 is the smallest. The vault settlement values of the tunnel under the three schemes are −42.13 mm, −46.89 mm, and −52.58 mm, respectively, and the haunch horizontal convergence value are −12.24 mm, −12.36 mm, and −12.60 mm, respectively. Although the three kinds of schemes cause large vault settlement values and on the basis of only considering the construction sequence, Case 1 is recommended for excavation.

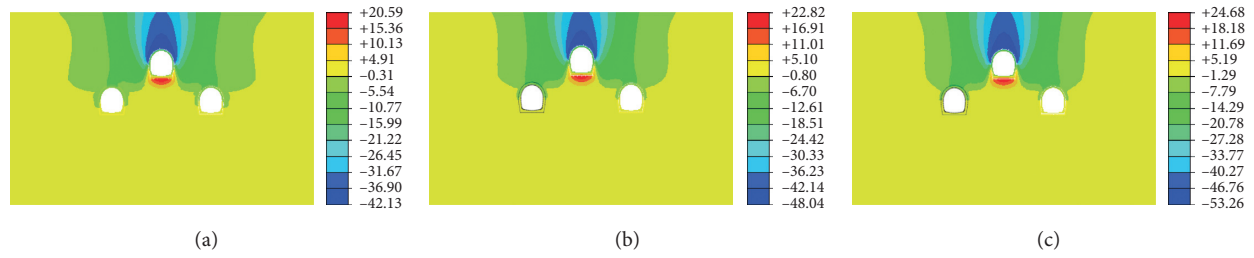*3.3.2. Surrounding Rock Stress.* Figures 6 and 7, respectively, show the maximum and minimum principal stress

(a)   (b)   (c)

FIGURE 4: The vertical displacement distribution cloud map of the surrounding rock (unit: mm). (a) Case 1. (b) Case 2. (c) Case 3.

(a)   (b)   (c)
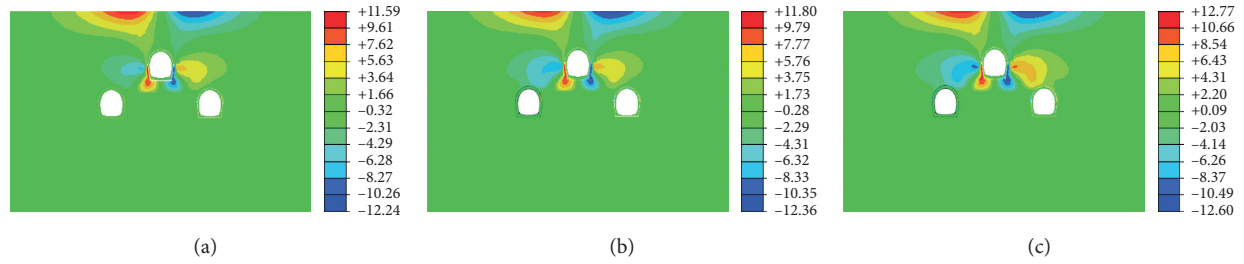
FIGURE 5: The horizontal displacement distribution cloud map of the surrounding rock (unit: mm). (a) Case 1. (b) Case 2. (c) Case 3.

TABLE 3: The vault settlement value of the tunnel and haunch horizontal convergence value under different construction schemes (unit: mm).

Monitoring points	P_1	P_2	P_3	S_1	S_2	S_3
Case 1	−6.81	−6.28	−42.13	−4.76	−4.24	−12.24
Case 2	−8.16	−9.18	−46.89	−4.72	−4.23	−12.36
Case 3	−10.32	−9.38	−52.58	−4.83	−4.26	−12.60

distribution cloud maps of the tunnel surrounding rock under different excavation schemes. It can be seen that the distribution law of the maximum and minimum principal stresses of the tunnel surrounding rock under the three excavation schemes are basically the same, and the excavation scheme has little influence on the stress of the tunnel surrounding rock. Through analysis, it can be seen that the maximum principal stresses of the tunnel surrounding rock under the three schemes are all distributed at the spandrel of the right tunnel, and the maximum values are 346.55 kPa, 346.75 kPa, and 352.03 kPa, respectively. The minimum principal stresses are all distributed at the haunch of the right tunnel, and the values are -1513.31 kPa, 1508.94 kPa, and 1556.29 kPa, respectively.

3.3.3. Surrounding Rock Stress. Figures 8 and 9 show the distribution cloud maps of the axial force and bending moment of the supporting structure under different excavation schemes, respectively. It can be seen from Figure 8 that the supporting structure under different excavation schemes is dominated by compressive stress, and the compressive stress distribution is relatively uniform. It can be seen from Figure 9 that the maximum positive bending moment and maximum negative bending moment of the supporting structure under different excavation schemes are located at the inverted arch and arch

foot of the middle line tunnel, respectively. It can be seen that there will be obvious uplift deformation at the inverted arch of the middle line tunnel. Through analysis, in Case 1, the maximum compressive stress on the tunnel haunch is 1280.98 kN, maximum compressive stress on the middle line tunnel is 454.21 kN, and maximum bending moment of the supporting structure is 336.72 kN m. In Case 2, the maximum compressive stress on the tunnel haunch is 1300.85 kN, maximum stress on the middle line tunnel is 454.21 kN, and maximum bending moment of the supporting structure is 337.12 kN m. In Case 3, the maximum stress on the tunnel haunch is 1313.40 kN, maximum stress of the middle tunnel is 468.74 kN, and maximum bending moment of the supporting structure is 337.43 kN m.

Through the above analysis, it can be seen that, under the same supporting conditions, the distribution of axial force and bending moment of the tunnel support structure under the three excavation schemes is basically the same, and the difference between the axial force value and bending moment value is small, that is, the three excavation schemes have little influence on the tunnel supporting structure.

3.3.4. Surface Settlement. Figure 10 shows the surface settlement curves under three excavation schemes. It can be seen that due to the close distance between the three tunnels, the surface settlement caused by the excavation of each
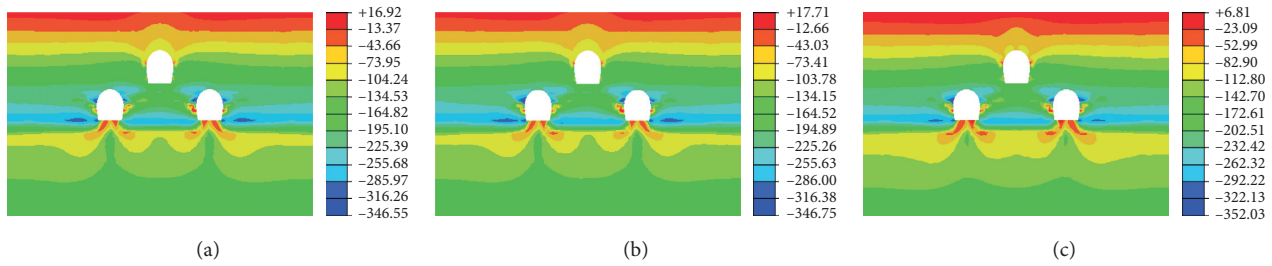
FIGURE 6: The maximum principal stress distribution cloud map of the surrounding rock (unit: kPa). (a) Case 1. (b) Case 2. (c) Case 3.
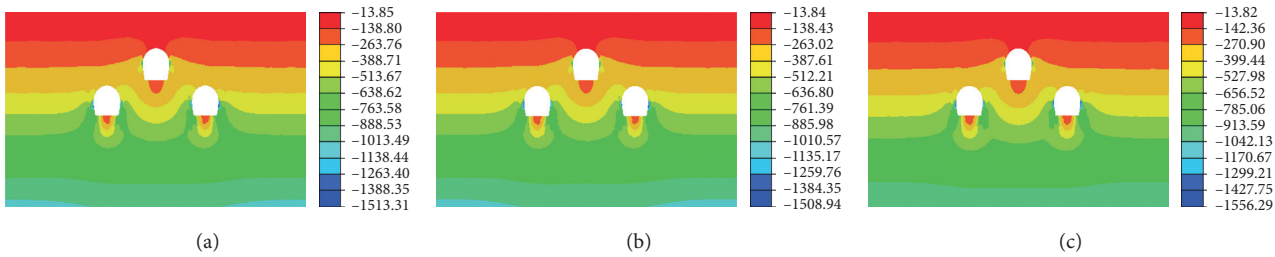

FIGURE 7: The minimum principal stress distribution cloud map of the surrounding rock (unit: kPa). (a) Case 1. (b) Case 2. (c) Case 3.
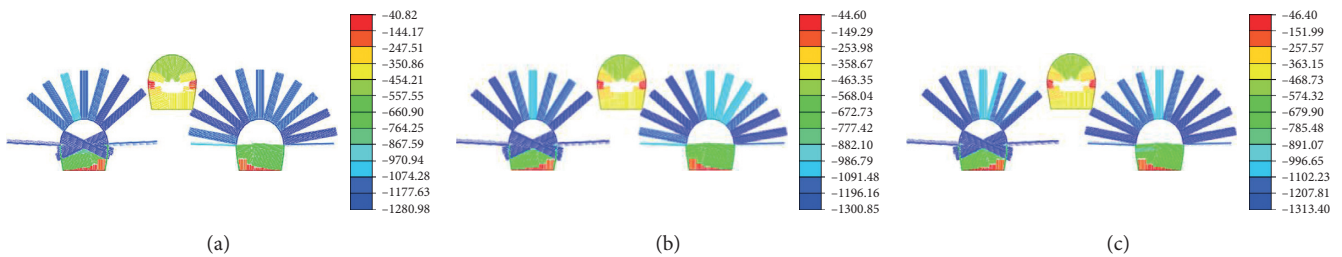

FIGURE 8: The axial force cloud map of the supporting structure (unit: kN). (a) Case 1. (b) Case 2. (c) Case 3.

tunnel gradually superimposes, resulting in the largest surface settlement in the middle part, and a "single peak" settlement curve with a small one on both sides and a large one on middle appears. In addition, it can be seen from Figure 10 that the width of the settlement tank under the three schemes is basically the same, and the first construction of the middle line tunnel in Cases 2 and 3 leads to the larger surface settlement. The maximum surface subsidence values under Cases 1–3 are 32.52 mm, 36.74 mm, and 41.55 mm in sequence. Although the surface settlement of the three cases exceeds the limit value of 30 mm, in comparison, Case 1 is more conducive to controlling the surface settlement during the construction process.

3.3.5. Plastic Zone Distribution.

Figure 11 shows the plastic zone distribution cloud map of the tunnel surrounding rock under three excavation schemes. It can be seen that, under the three excavation schemes, the plastic zone of the surrounding rock of the tunnel is mainly distributed at the spandrel, haunch, arch foot, and inverted arch of the middle line tunnel. There is basically no plastic zone distribution

near the left and right tunnels. Through the comparative analysis of the distribution of the tunnel plastic zone under the three excavation schemes, it can be found that the plastic zone caused by Case 1 is slightly smaller than the size of the surrounding rock plastic zone caused by the other two schemes. Therefore, from the perspective of considering plastic zone, the preferred choice for tunnel excavation is Case 1.

Through comparative analysis of the displacement, internal force, surface settlement, and plastic zone distribution of the tunnel surrounding rock and support system under the three excavation schemes, it can be seen that Case 1, namely, firstly excavate the right tunnel, then excavate the left tunnel, and finally excavating the middle line tunnel is the most effective way to control the deformation of the surrounding rock and the stress and shape change of the supporting structure. In addition, the plastic zone of the surrounding rock caused by Case 1 is smaller than the plastic zones caused by Cases 2 and 3. On comprehensive comparison, it is recommended to carry out on-site construction in accordance with Case 1, namely, the excavation sequence of right line tunnel ⟶ left line tunnel ⟶ middle line
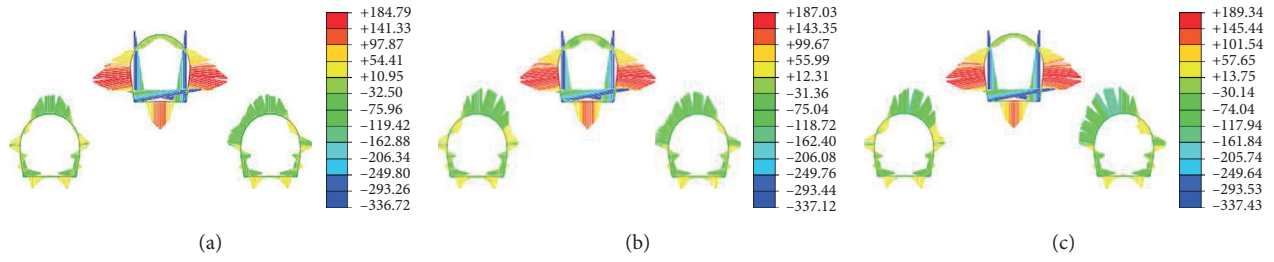
FIGURE 9: The bending moment cloud map of the supporting structure (unit: kN·m). (a) Case 1. (b) Case 2. (c) Case 3.

tunnel. However, the surface settlement under the three schemes all exceeded the limit value of 30 mm, which cannot guarantee the safety of expressway traffic. Therefore, it is necessary to adopt advanced small pipe grouting pre-reinforcement measures for the left, middle, and right tunnels and use steel tube concrete piles to reinforce the base of the middle tunnel in order to improve the stability of the tunnel surrounding rock.

4. Control Countermeasures for the Construction of Triangular Three-Line Metro Tunnels Undercrossing the Expressway

The advanced small pipe grouting is the most commonly used prereinforcement treatment method in the construction of shallow burying and undercutting. The principle is that the surrounding rock in a certain range in front of the tunnel is excavated and drilled at a certain inclination angle, and a small pipe with holes is installed or a small pipe with holes is directly drilled, and then, the surrounding rock is pressure injected through the small pipe cementing slurry. After the grout is hardened, on the one hand, the surrounding rock can be cemented into a hole, which improves the self-stability of the surrounding rock and plays a role in reinforcement. On the other hand, it plugs the fissures of the surrounding rock and plays a role in blocking water. Combining the actual situation of the project of Chongqing metro line 6 underpassing through the expressway around the city, according to the design, the soil in the 180° area of the arch of the three tunnels is driven into a Φ42 double-row advanced small pipe. The layout of the advanced small pipe is shown in Figure 12, and as indicated in Figure 12, the relevant parameters are given in Table 4.

In order to reduce the risk of inverted arch uplift and to ensure the operational safety of the tunnel, the steel tube concrete piles are adopted to strengthen the soft foundation of the tunnel inverted arch during the construction process of the Chongqing metro line 6. The on-site steel pipe piles are made of 406*5.6 mm steel pipes, 6Φ20 steel cages are installed, and C40 waterproof concrete is poured. The length of the steel pipe piles is about 12 m, and the depth of the rock (sandstone) embedded in the actual construction is guaranteed to be 2 m. Figures 13 and 14, respectively, show the reinforced cross-section and plan layout of concrete-filled steel tube piles.

4.1. Numerical Model and Parameters. The numerical model after reinforcement is established on the basis of the model in Section 3. The physical and mechanical parameters of the

ground and supporting structure are shown in Tables 1 and 2. The selection of the constitutive model and other model conditions are the same as in Section 3, and the numerical model is divided into 1973 nodes and 2095 elements.

At present, the effect of advanced presupport can be equivalently analyzed by changing the physical and mechanical parameters of the surrounding rock in a certain area. The thickness of the grouting reinforcement zone can be calculated by Equation (2), taking 0.6 m. The physical and mechanical parameters of the surrounding rock after grouting can be determined by Equation (3). The final parameter determination results are shown in Table 5.

$$D = 2\left[R^2 - \left(\frac{S}{2}\right)^2\right]^{0.5}, \tag{2}$$

where D is the thickness of the reinforcement ring, R is the grout diffusion radius, taking S (0.6 ∼ 0.8), and S is the distance between adjacent grouting holes.

$$E = \frac{E_1 I_1 + k_w E_2 I_2}{I_1 + I_2}, \tag{3}$$

where E is equivalent stiffness (GPa), E_1 is steel tube elastic modulus (GPa), I_1 is steel tube moment of inertia (m^4), E_2 is steel tube filled with elastic modulus of mortar (GPa), I_2 is moment of inertia of mortar filled in steel pipe (m^4), and k_w is considered the coefficient of mortar stiffness reduction caused by mortar cracking, and 0.6 is taken.

When simulating steel pipe piles in finite element software, the interaction between the pile circumference, pile tip, and rock and soil should be considered. In this paper, the 1D beam element is used to simulate a concrete-filled steel tube pile, and a pile element is built around the steel tube pile to simulate the contact between the pile circumference and rock and soil, with a pile end element established at the bottom of the beam element to simulate the interaction between the pile end and rock and soil. Table 6 shows the relevant parameters of concrete-filled steel tube piles.

4.2. Reinforcement Optimization Scheme Design. It can be seen from Section 3 that, compared with Cases 2 and 3, the excavation sequence of Case 1 is more reasonable to ensure the stability of the surrounding rock of the triangularly distributed three-line metro tunnels. Therefore, this section optimizes the reinforcement scheme on the basis of Case 1. Taking the right tunnel as an example, the
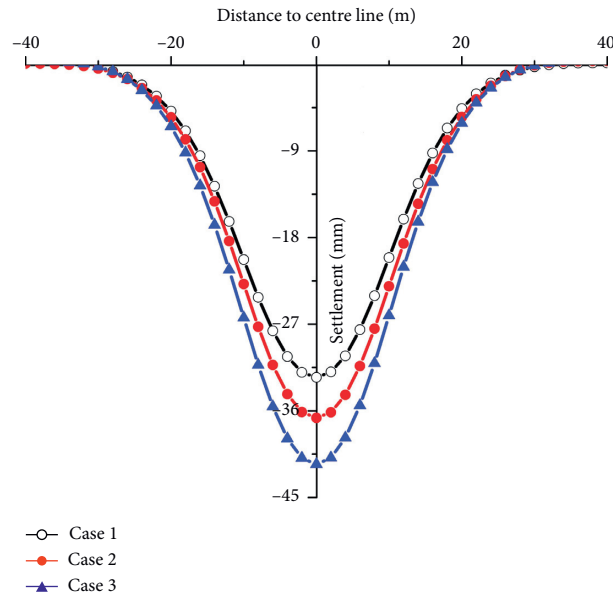
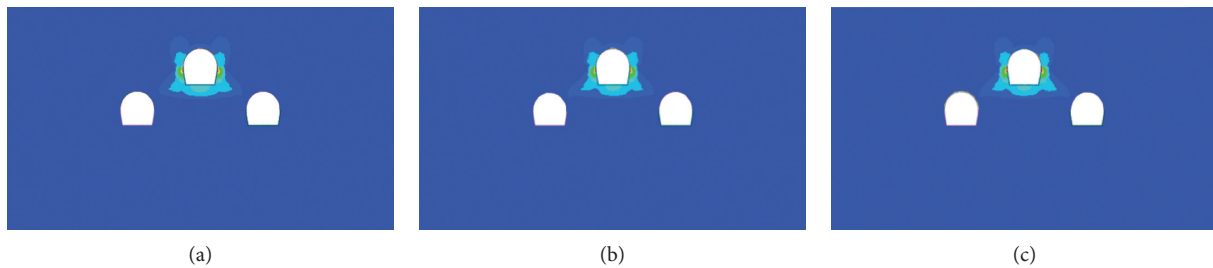FIGURE 10: Comparison of the surface settlement.

FIGURE 11: The cloud map of plastic zone distribution. (a) Case 1. (b) Case 2. (c) Case 3.

specific reinforcement sequence is given as follows (as shown in Figure 15): (1) reinforce area by using advanced small pipe grouting; (2) excavate pilot tunnel and implement primary support; (3) excavate the core soil of the right hole and construct the middle partition; (4) excavate pilot tunnel , construct primary support, and remove the middle partition; (5) construct the secondary lining and complete the construction of the right tunnel. In accordance with the above sequence, according to Case 1, the construction of the left tunnel and middle tunnel were completed in turn.

4.3. Analysis of Numerical Simulation Results

4.3.1. Deformation of the Surrounding Rock and Supporting Structure. Figures 16 and 17, respectively, show the vertical and horizontal displacement cloud maps of the tunnel surrounding rock before and after the reinforcement scheme is adopted. It can be seen that, after the tunnel excavation is completed, the surrounding rock deformation distribution law is basically the same before and after the reinforcement scheme is adopted. Due to the

poor nature of the surrounding rock in the middle line tunnel, the vault settlement and inverted arch uplift are more obvious than those of the left and right line tunnels. The maximum settlement occurred at the vault of the middle line tunnel, with the maximum values of −42.13 mm and -20.17 mm, respectively. The maximum uplift occurred at the inverted arch of the tunnel, with the maximum values of 20.59 mm and 18.50 mm, respectively. The maximum horizontal displacements all appear on the right side of the middle line tunnel, in the negative direction along the X-axis, and the maximum horizontal displacements are 12.36 mm and 13.08 mm, respectively. It can be seen from the calculation results that the reinforcement scheme has a significant control effect on the deformation of the tunnel surrounding rock.

In order to study the influence of the reinforcement scheme on the initial support deformation of the tunnel, the settlement of the tunnel vault and horizontal convergence of the arch waist were selected as reference values for analysis (the monitoring points are the same as in Section 3). Table 7 shows the settlement value of the tunnel vault and level of the arch waist before and after
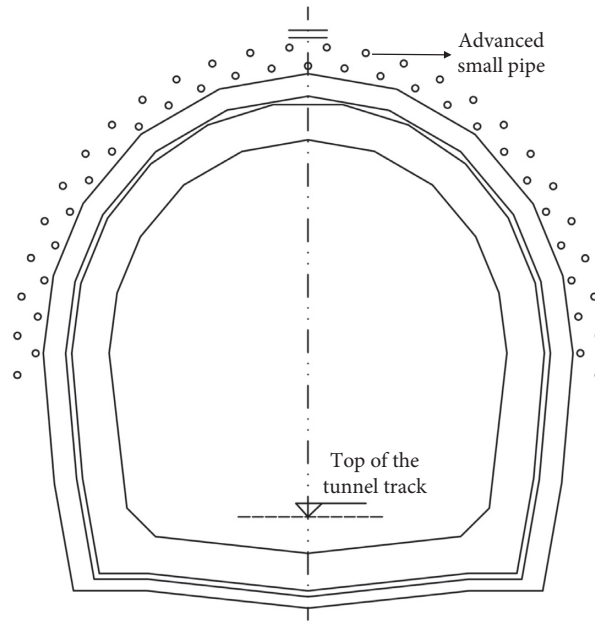
FIGURE 12: The layout of the advanced small pipes.

TABLE 4: Parameters of the advanced small pipes.

Small pipes	Length (mm)	Longitudinal spacing (mm)	Circumferential spacing (mm)	Extrapolation angle (°)	Grouting hole	Notes
Inner layer	5	2.5	0.4	40	Plum blossom arrangement with 0.5 m spacing	Chemical grouting
Outer layer	3.5	2.0	0.3	10~15		

the reinforcement scheme. It can be seen from Table 7 that the deformation of the supporting structure is very different before and after the reinforcement scheme is adopted. The deformation of the supporting structure after the reinforcement scheme is adopted and is significantly smaller than that without the reinforcement scheme. After adopting the reinforcement scheme at the same time, the maximum deformation can be controlled within 30 mm.

4.3.2. Surrounding Rock Stress. Figures 18 and 19 show the distribution cloud maps of the maximum and minimum principal stress of the tunnel surrounding rock before and after reinforcement measures are adopted. It can be seen that there is no obvious difference between the maximum principal stress of the surrounding rock after the tunnel excavation is completed before and after the use of reinforcement measures, but the minimum principal stress has changed significantly. Before adopting the reinforcement scheme, the maximum principal stress and minimum principal stress of the surrounding rock appeared at the arch shoulder and haunch of the right tunnel, respectively, and the values are 346.55 kPa and −1513.31 kPa, respectively; after the reinforcement

scheme is adopted, the maximum principal stress of the surrounding rock appears at the vaults of the left and right tunnels, and the minimum principal stress appears at the haunch of the right tunnel and the values are 333.14 kPa and −1886.04 kPa, respectively.

4.3.3. Supporting Structure Force. Figures 20 and 21 show the distribution cloud maps of the axial force and bending moment of the supporting structures before and after the reinforcement scheme is adopted. It can be seen that, before and after the reinforcement scheme is adopted, the axial force of the supporting structure is mainly pressure, and the pressure distribution is relatively uniform. The maximum positive bending moment of the supporting structure is located at the inverted arch of the middle line tunnel, and the maximum negative bending moment is located at the arch foot of the middle line tunnel, indicating that there will be obvious uplift deformation at the inverted arch. The analysis shows that, before the reinforcement scheme is adopted, the maximum pressure of the tunnel appears at the haunch of the left and right tunnels, and its value is 1280.98 kN. The maximum pressure on the middle line tunnel is 454.21 kN, and the maximum bending moment of the supporting structure is

Φ406 × 5.6 mm
concrete pile

The distance between the
piles are 1.5 × 1.0 m

The length inserted into
the sandstone is longer
than 2 m

631   1100   1100   1100   631
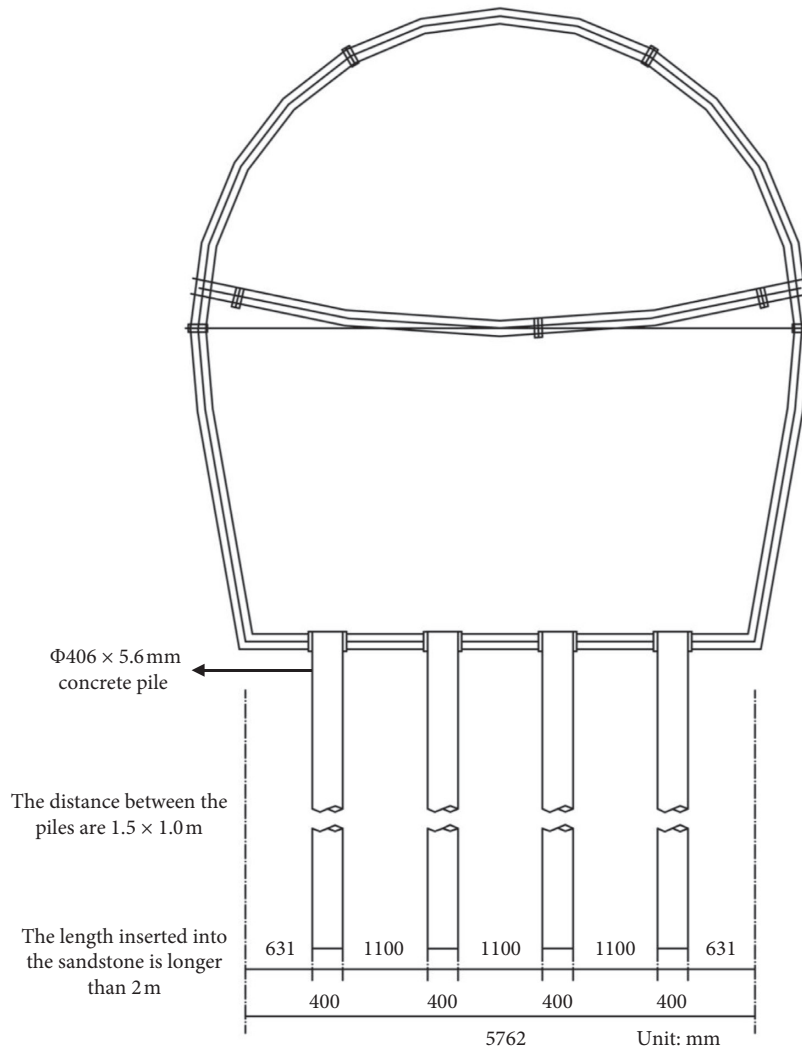
400   400   400   400

5762   Unit: mm

FIGURE 13: The reinforced section view of the steel tube concrete pile.

336.72 kN m. After the reinforcement scheme is adopted, the maximum pressure of the tunnel appears at the haunch of the left and right tunnels, with a value of 1071.39 kN. The maximum pressure on the middle line tunnel is 342.50 kN, and the maximum bending moment of the supporting structure is 328.34 kN·m. The above phenomenon shows that the reinforcement scheme can play a good control effect on the axial force and bending moment of the supporting structure.

4.3.4. Surface Settlement. Figure 22 shows the surface settlement curves before and after the reinforcement scheme is adopted. It can be seen that the surface settlement curves before and after adopting the reinforcement scheme still show a "single peak" settlement curve with small sides on both sides and large sides in the middle. Moreover, the width of the settlement tank before and after the reinforcement scheme is basically the same. The maximum settlement value after reinforcement is 16.47 mm, which is close to the surface settlement value of 18.31 mm after the tunnel excavation is completed after 170 days, and is much smaller than that before the reinforcement measures (32.52 mm). Therefore, the reinforcement scheme in this section can effectively control the surface settlement value within the limit value of 30 mm, indicating that the reinforcement scheme has an obvious control effect on the surface settlement during tunnel construction.

4.3.5. Plastic Zone Distribution. Figure 23 shows the plastic zone distribution cloud map of the tunnel surrounding rock before and after the reinforcement scheme is adopted. It can be seen that, before and after the reinforcement scheme is adopted, the plastic zones are mainly concentrated at the arch shoulder, haunch, arch foot, and inverted arch of the middle line tunnel. However, compared with no reinforcement scheme, the plastic zone distribution area of the arch shoulder is greatly reduced after the reinforcement plan is adopted, indicating that the reinforcement scheme has a significant inhibitory effect on the development of the plastic zone of the surrounding rock.
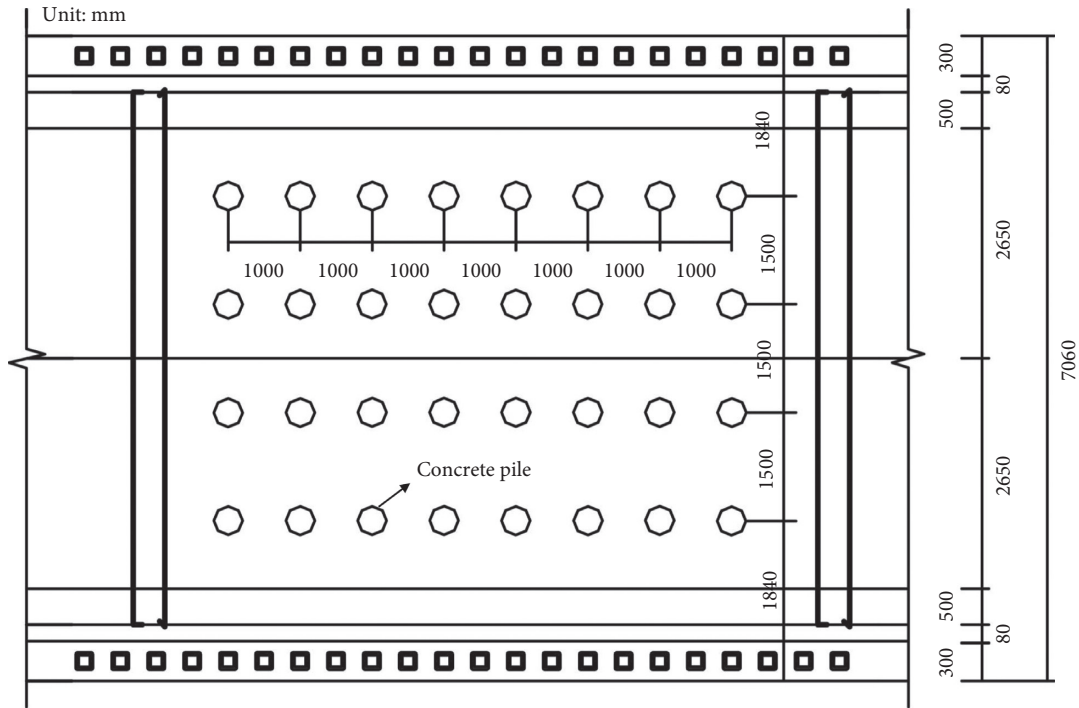
Figure 14: The layout plan of concrete-filled steel tube piles.

Table 5: Physical and mechanical parameters of the surrounding rock in the grouting reinforcement area.

Type	Elastic modulus (MPa)	Internal friction angle (°)	Cohesion (kPa)	Poisson's ratio
Advanced small-pipe grouting reinforcement area	103.55	23.5	108	0.2

Table 6: Numerical simulation parameters of concrete-filled steel tube piles.

Type	Shear stress (kPa)	Shear stiffness modulus (kN·m^{-3})	Normal stiffness modulus (kN·m^{-3})	Pile-end bearing capacity (kN)	Bulk density (kN·m^{-3})	Elastic modulus (MPa)	Poisson's ratio
Pile unit	306	48465	126000	-	-	-	-
Pile end unit	-	-	-	300	-	-	-
Concrete-filled steel tube pile	-	-	-	-	23	3000	0.2

Through the above analysis, it can be seen that the use of advanced small pipe grouting and steel tube concrete piles to strengthen the control measures of the tunnel base in the middle tunnel not only is conducive to controlling the deformation and force of the surrounding rock and supporting structure but also the deformation value is controlled within the specified range. Moreover, the distribution range of the plastic zone after the reinforcement is smaller. Therefore, for this project, it is recommended to excavate according to Case 1, namely, in the sequence of right line tunnel ⟶ left line tunnel ⟶ middle line tunnel. At the same time, the site construction was carried out in cooperation with the control plan of advanced small pipe grouting and steel tube concrete piles to strengthen the base of the middle line tunnel.
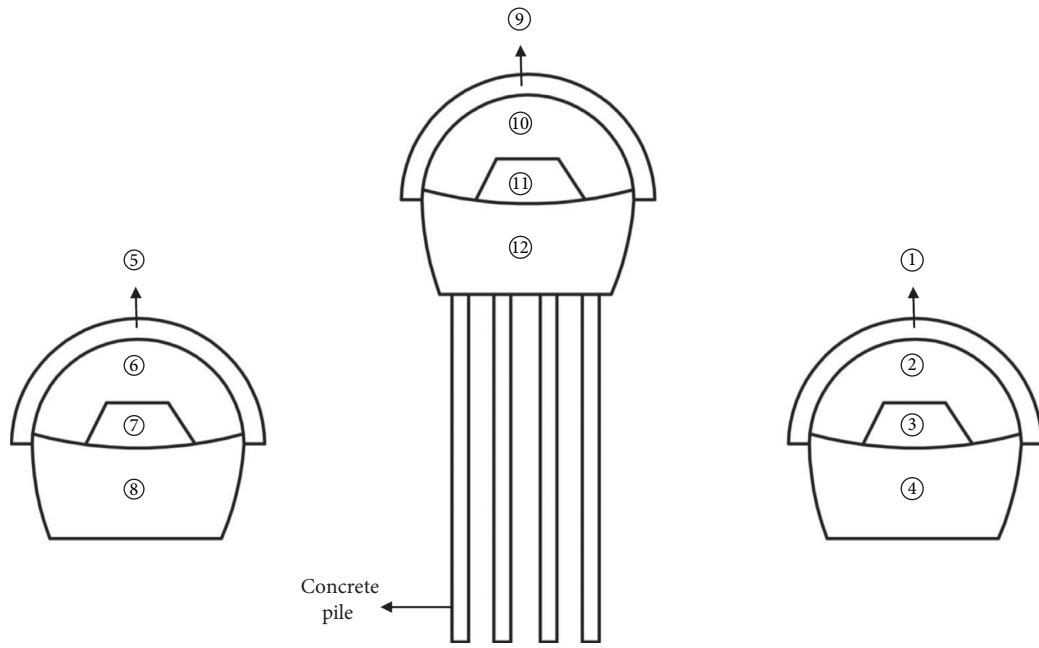
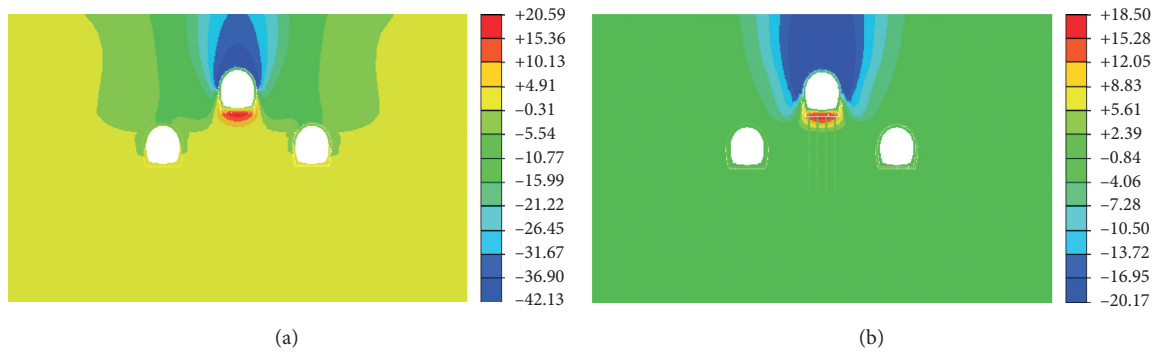FIGURE 15: Tunnel reinforcement construction sequence.

(a)   (b)

FIGURE 16: The vertical displacement distribution cloud map of the surrounding rock (unit: mm). (a) Not reinforced. (b) Reinforced.

(a)   (b)
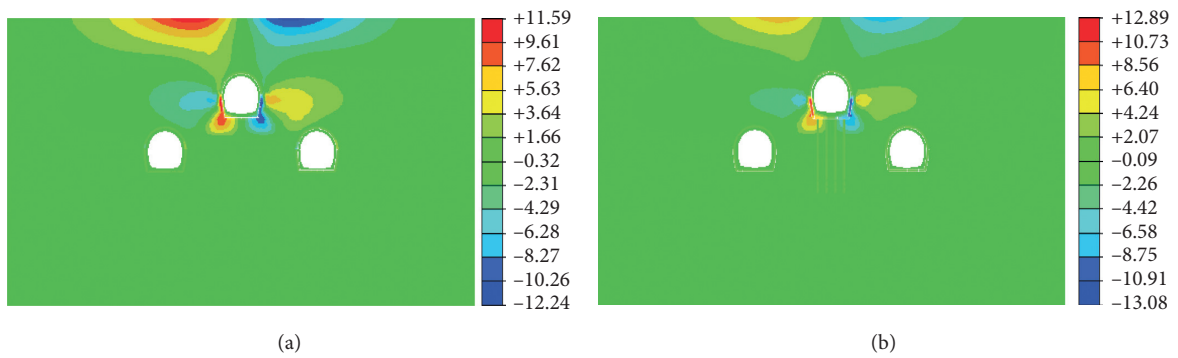
FIGURE 17: The horizontal displacement distribution cloud map of the surrounding rock (unit: mm). (a) Not reinforced. (b) Reinforced.

TABLE 7: The vault settlement value of the tunnel and haunch horizontal convergence value under different construction schemes (unit: mm).

Feature points	P_1	P_2	P_3	S_1	S_2	S_3
Before reinforcement	−6.81	−6.28	−42.13	−4.56	−4.14	−12.24
After reinforcement	−1.50	−1.51	−20.17	−1.21	−1.04	−13.08

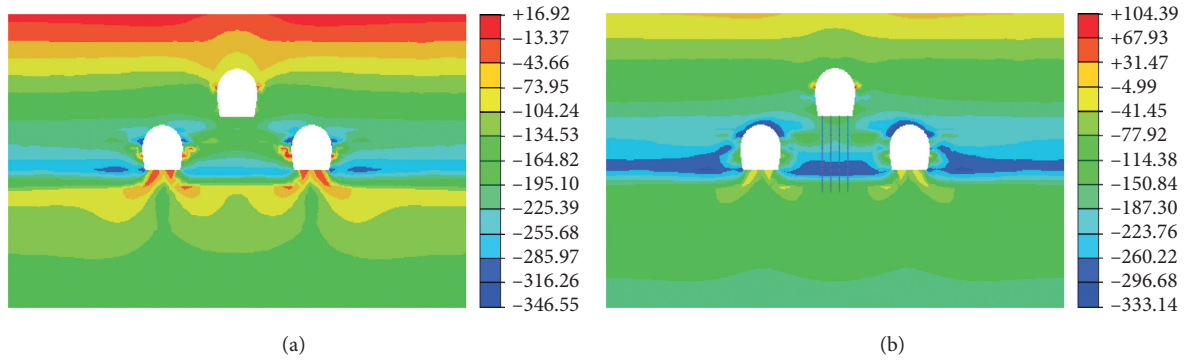(a)   (b)

FIGURE 18: The maximum principal stress cloud map of the surrounding rock (unit: kPa). (a) Not reinforced. (b) Reinforced.

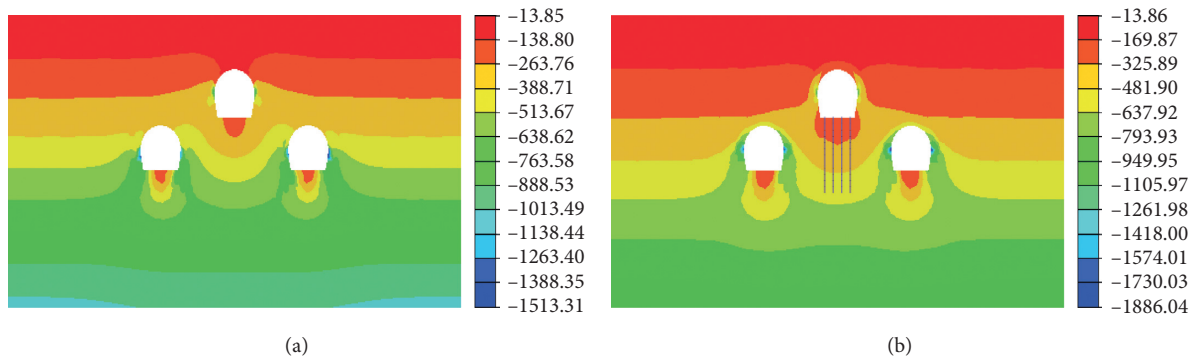(a)   (b)

FIGURE 19: The minimum principal stress cloud map of the surrounding rock (unit: kPa). (a) Not reinforced. (b) Reinforced.
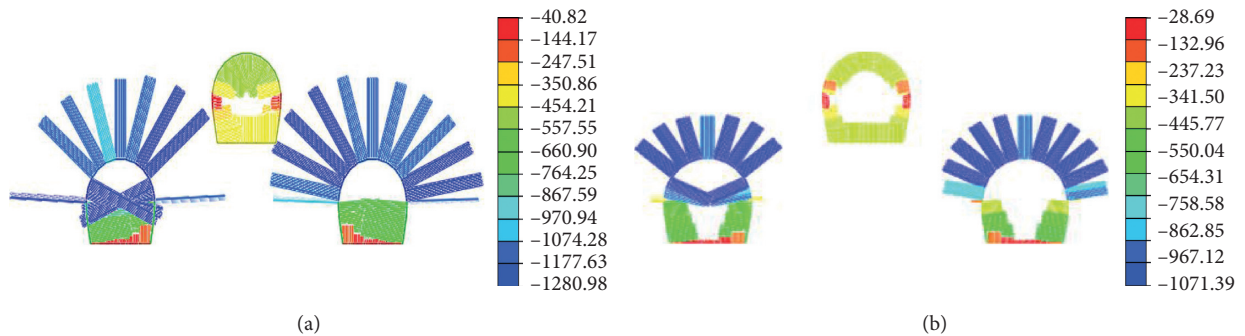

(a)   (b)

FIGURE 20: The axial force cloud map of the supporting structure (unit: kN). (a) Not reinforced. (b) Reinforced.

(a)   (b)
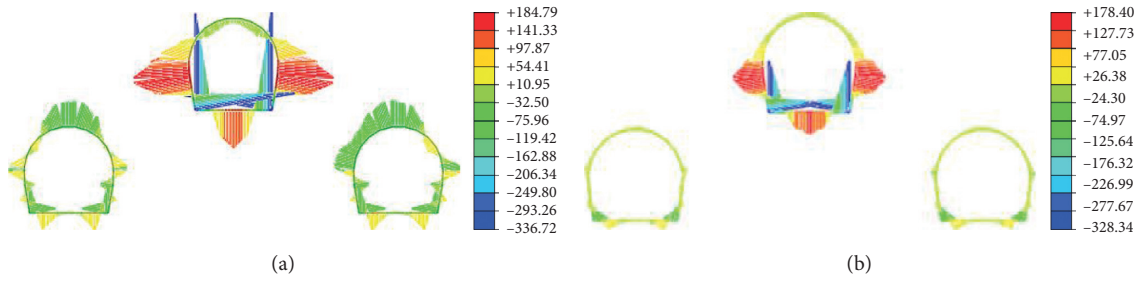
FIGURE 21: The bending moment cloud map of the supporting structure (unit: kN·m). (a) Not reinforced. (b) Reinforced.
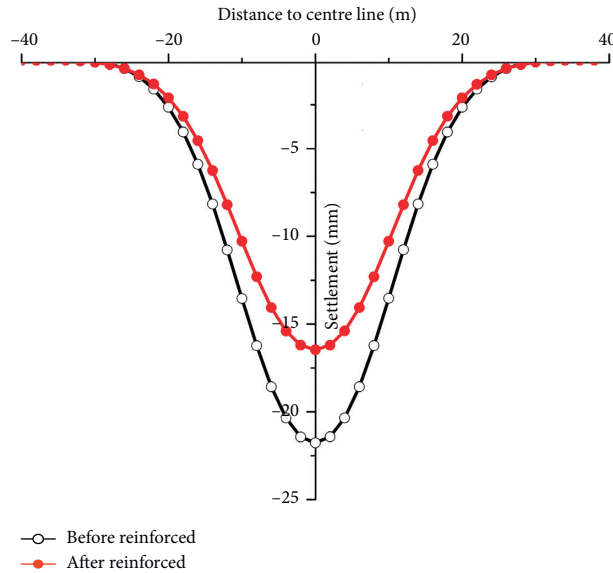

FIGURE 22: Comparison of the surface settlement before and after the reinforcement scheme is adopted.
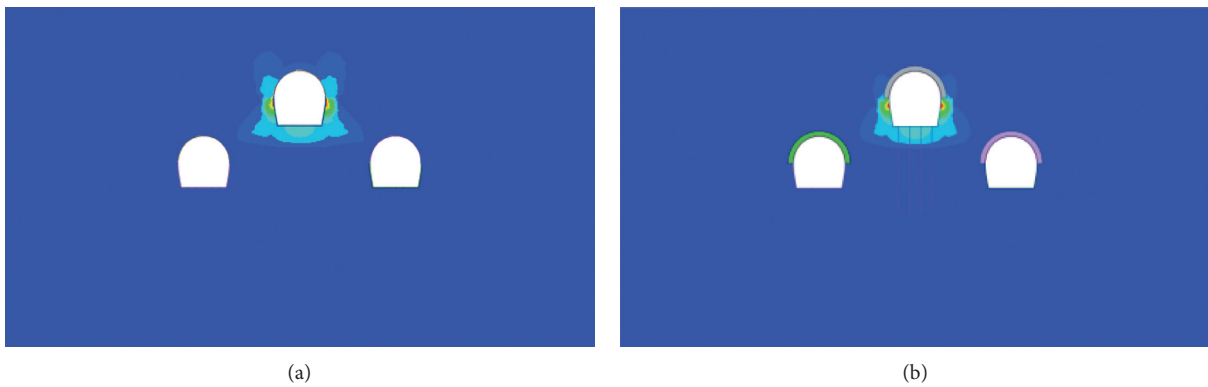

(a)   (b)

FIGURE 23: The plastic zone distribution cloud map before and after reinforced. (a) Not reinforced. (b) Reinforced.

5. Conclusions

In this paper, relying on the project of Chongqing metro tunnel line 6 underpassing through the expressway around the city, numerical simulation methods are used to study the surrounding rock deformation, surface settlement, and stress distribution of the supporting structure of the three-line metro tunnels with a triangular distribution under different excavation sequences, and the optimal excavation sequence is determined. On this basis, the control measure

for strengthening the three-line tunnels with advanced small pipe grouting and reinforcing the middle tunnel with concrete-filled steel tube piles are proposed. The main conclusions obtained are as follows:

(1) Numerical simulation results under three different excavation schemes show that the excavation sequence of Case 1 (right line tunnel ⟶ left line tunnel ⟶ middle line tunnel) is effective in controlling the deformation of surrounding rock, supporting structure stress, and surface settlement. The control effects of the surface settlement and development of plastic zone are the best, which helps ensure the rapid and safe construction of metro tunnels.

(2) Although the excavation sequence of Case 1 is conducive to ensuring the safe construction of the triangularly distributed three-line metro tunnel, the surface settlement exceeds the limit value (30 mm), which is not conducive to the safety of the upper expressway. Therefore, in order to reduce the impact of metro tunnel construction on the upper expressway, a treatment method is proposed to pre-reinforce the three tunnels by grouting with small pipes in advance, and to use concrete-filled steel tube piles to strengthen the base of the middle line tunnel.

(3) The numerical simulation of the excavation process of the triangular-distributed three-line metro tunnel with and without the reinforcement scheme is carried out. The results show that the use of reinforcement schemes can effectively control surface settlement, tunnel surrounding rock deformation, support structure stress, and plastic zone development, which is conducive to the safety of tunnel construction and safe operation of the upper expressway.

Data Availability

The data used to support the findings of this study are available from the corresponding author upon request.

Conflicts of Interest

The authors declare that they have no conflicts of interests.

Acknowledgments

References

[1] H. Wu, Y. J. Zhong, W. Shi, X. H. Shi, and T. Liu, "Experimental investigation of ground and air temperature fields of cold-region road tunnels in NW China," *Advances in Civil Engineering*, vol. 2020, Article ID 4732490, 13 pages, 2020.

[2] W. C. Cheng, G. Li, D. E. L. Ong, S. L. Chen, and J. C. Ni, "Modelling liner forces response to very close-proximity tunnelling in soft alluvial deposits," *Tunnelling and Underground Space and Technology*, vol. 103, Article ID 103455, 2020.

[3] Z. F. Chu, Z. J. Wu, Q. S. Liu, and B. G. Liu, "Analytical solutions for deep-buried lined tunnels considering longitudinal discontinuous excavation in rheological rock mass," *Journal of Engineering Mechanics*, vol. 146, no. 6, Article ID 04020047, 2020.

[4] Z. P. Song, J. C. Mao, X. X. Tian, Y. W. Zhang, and J. B. Wang, "Optimization analysis of controlled blasting for passing through houses at close range in super-large section tunnels," *Shock and Vibration*, vol. 2019, Article ID 1941436, 16 pages, 2019.

[5] K. Wu and Z. S. Shao, "Visco-elastic analysis on the effect of flexible layer on mechanical behavior of tunnels," *International Journal of Applied Mechanics*, vol. 11, no. 3, Article ID 1950027, 2019.

[6] H. P. Lai, H. W. Zheng, R. Chen, Z. Kang, and Y. Liu, "Settlement behaviors of existing tunnel caused by obliquely under-crossing shield tunneling in close proximity with small intersection angle," *Tunnelling and Underground Space and Technology*, vol. 97, Article ID 103258, 2020.

[7] K. Wu and Z. S. Shao, "Study on the effect of flexible layer on support structures of tunnel excavated in viscoelastic rocks," *Journal of Engineering Mechanics*, vol. 145, no. 10, Article ID 04019077, 2019.

[8] Z. P. Song, X. X. Tian, Q. Liu, Y. W. Zhang, H. Li, and G. N. Zhou, "Numerical analysis and application of the construction method for small interval tunnel in the turn line of metro," *Science Progress*, vol. 103, no. 3, Article ID 0036850420932067, 2020.

[9] J. B. Wang, Q. Zhang, Z. P. Song, and Y. W. Zhang, "Experimental study on creep properties of salt rock under long-period cyclic loading," *International Journal of Fatigue*, vol. 143, Article ID 106009, 2021.

[10] J. Su, Q. Fang, D. L. Zhang, X. K. Niu, X. Liu, and Y. M. Jie, "Bridge responses induced by adjacent subway station construction using shallow tunneling method," *Advances in Civil Engineering*, vol. 2018, Article ID 8918749, 16 pages, 2018.

[11] K. Wu, Z. S. Shao, S. Qin, N. N. Zhao, and H. K. Hu, "Analytical-based assessment of effect of highly deformable elements on tunnel lining within viscoelastic rocks," *International Journal of Applied Mechanics*, vol. 12, no. 3, Article ID 2050030, 2020.

[12] Z. Zhang and M. Huang, "Geotechnical influence on existing subway tunnels induced by multiline tunneling in Shanghai soft soil," *Computers and Geotechnics*, vol. 56, pp. 121–132, 2014.

[13] H. F. Lu, "Stress and displacement analysis of aerial oil and gas pipelines: a case study of Lantsang tunnel crossing project," *Journal of Engineering Research*, vol. 3, no. 3, pp. 141–156, 2015.

[14] B. Liu, D. Xi, and P. Xu, "Study on the interaction of metro shield tunnel construction under-crossing the existing Longhai railway," *Geotechnical and Geological Engineering*, vol. 38, no. 2, pp. 2159–2168, 2020.

[15] J.-S. Chung, J.-Y. Choi, and J.-H. Lee, "A study on the stability of existing subway tunnel due to construction of new underpass," *Journal of the Korean Society of Safety*, vol. 31, no. 2, pp. 57–63, 2016.

[16] H. F. Xing, F. Xiong, and J. M. Wu, "Effects of pit excavation on an existing subway station and preventive measures,"

Journal of Performance of Constructed Facilities, vol. 30, no. 6, Article ID 04016063, 2016.

[17] X. Zhang, C. P. Zhang, and J. C. Wang, "Effect of closely spaced twin tunnel construction beneath an existing subway station: a case study," *Journal of Testing and Evaluation*, vol. 46, no. 4, pp. 1559–1573, 2018.

[18] H. P. Lai, X. Zhao, Z. Kang, and R. Chen, "A new method for predicting ground settlement caused by twin-tunneling under-crossing an existing tunnel," *Environmental Earth Sciences*, vol. 76, no. 21, 726 pages, 2017.

[19] D. Jin, D. Yuan, X. Li, and H. Zheng, "Analysis of the settlement of an existing tunnel induced by shield tunneling underneath," *Tunnelling and Underground Space Technology*, vol. 81, pp. 209–220, 2018.

[20] K. Wu, W. Zhang, H. T. Wu, Y. J. Wang, and Z. L. Liu, "Study of impact of metro station side-crossing on adjacent existing underground structure," *Journal of Intelligent and Fuzzy Systems*, vol. 31, no. 4, pp. 2291–2298, 2016.

[21] Z. Zhou, Y. Chen, Z. Z. Liu, and L. W. Miao, "Theoretical prediction model for deformations caused by construction of new tunnels undercrossing existing tunnels based on the equivalent layered method," *Computers and Geotechnics*, vol. 123, Article ID 103565, 2020.

[22] P. Castaldo, M. Calvello, and B. Palazzo, "Probabilistic analysis of excavation-induced damages to existing structures," *Computers and Geotechnics*, vol. 53, pp. 17–30, 2013.

[23] Z. P. Song, Y. Cheng, X. X. Tian, J. B. Wang, and T. T. Yang, "Mechanical properties of limestone from Maixi tunnel under hydro-mechanical coupling," *Arabian Journal of Geosciences*, vol. 13, no. 11, 402 pages, 2020.

[24] J. B. Wang, Q. Zhang, Z. P. Song, Y. W. Zhang, and X. R. Liu, "Mechanical properties and damage constitutive model for uniaxial compression of salt rock at different loading rates," *International Journal of Damage Mechanics*, vol. 30, Article ID 20048, 2021.

[25] W. C. Cheng, G. Li, N. N. Liu, J. Xu, and S. Horpibulsuk, "Recent massive incidents for subway construction in soft alluvial deposits of Taiwan: a review," *Tunnelling and Underground Space and Technology*, vol. 96, Article ID 103178, 2020.

[26] K. Wu, Z. S. Shao, S. Qin, W. Wei, and Z. Chu, "A critical review on the performance of yielding supports in squeezing tunnels," *Tunnelling and Underground Space Technology*, vol. 114, no. 1, 2021.

[27] Z. Chu, Z. Wu, B. Liu, and Q. Liu, "Coupled analytical solutions for deep-buried circular lined tunnels considering tunnel face advancement and soft rock rheology effects," *Tunnelling and Underground Space Technology*, vol. 94, Article ID 103111, 2019.

[28] J. B. Wang, X. R. Liu, Z. P. Song, J. Q. Guo, and Q. Q. Zhang, "A creep constitutive model with variable parameters for thenardite," *Environmental Earth Sciences*, vol. 75, no. 6, 979 pages, 2016.

[29] B. Hu, M. Sharifzadeh, X. T. Feng, W. Guo, and R. Talebi, "Roles of key factors on large anisotropic deformations at deep underground excavations," *International Journal of Mining Science and Technology*, vol. 31, no. 2, 2021.

[30] J. Wang, Q. Zhang, Z. Song, and Y. Zhang, "Creep properties and damage constitutive model of salt rock under uniaxial compression," *International Journal of Damage Mechanics*, vol. 29, no. 6, pp. 902–922, 2020.

[31] K. Wu, Z. S. Shao, and S. Qin, "An analytical design method for ductile support structures in squeezing tunnels," *Archives of Civil and Mechanical Engineering*, vol. 20, 91 pages, 2020.

[32] R. Liang, T. Xia, Y. Hong, and F. Yu, "Effects of above-crossing tunnelling on the existing shield tunnels," *Tunnelling and Underground Space Technology*, vol. 58, pp. 159–176, 2016.

[33] H. Li, E. L. Ma, J. X. Lai et al., "Tunnelling induced settlement and treament techniques for a loess metro in Xi'an," *Advances in Civil Engineering*, vol. 2020, Article ID 1854813, 20 pages, 2020.

[34] W. C. Cheng, G. Li, A. N. Zhou, and J. Xu, "Rethinking the water leak incident of tunnel Luo09 to prepare for a challenging future," *Advances in Civil Engineering*, vol. 2019, Article ID 4695987, 11 pages, 2019.

[35] X. G. Li and D. J. Yuan, "Response of a double-decked metro tunnel to shield driving of twin closely under-crossing tunnels," *Tunnelling and Underground Space Technology*, vol. 28, pp. 18–30, 2012.

[36] J.-B. Wang, X.-R. Liu, X.-J. Liu, and M. Huang, "Creep properties and damage model for salt rock under low-frequency cyclic loading," *Geomechanics and Engineering*, vol. 7, no. 5, pp. 569–587, 2014.

[37] T. Liu, Y. Xie, Z. H. Feng, Y. B. Luo, K. Wang, and W. Xu, "Better understanding the failure modes of tunnels excavated in the boulder-cobble mixed strata by distinct element method," *Engineering Failure Analysis*, vol. 116, Article ID 104712, 2020.